A Cascaded Heterogeneous Equivalent Network for Evaluating RF-induced Hazards on Active Implantable Medical Devices

Jingshen Liu, *Student Member, IEEE,* Yu Wang, Ran Guo, Qingyan Wang, Jianfeng Zheng, *Member,* Krishina Kurpad, Wolfgang Kainz, *Member, IEEE, and* Ji Chen, *Senior Member, IEEE*

***Abstract*—This paper presents a cascaded heterogeneous equivalent network for the evaluation of radiofrequency (RF) induced safety hazards on electrically long active implantable medical devices (AIMDs) exposed to magnetic resonance imaging (MRI) systems. AIMDs in a highly heterogeneous human body are represented by cascaded transmission line models consisting of segments with different values of effective wavenumbers and characteristic impedances. Two terminations, implantable pulse generator (IPG) and lead-tip are modeled as lumped elements. Methods to extract values for lead-tip impedance, IPG impedance, wavenumber, and characteristic impedance of the AIMDs are proposed and validated through numerical simulations and experimental investigations. Based on these values, one can build up a unique AIMD model along each implanted trajectory inside human body models. The developed models can be used to accurately evaluate the RF-induced voltage and heating for each implantation scenario.**

***Index Terms*—Active implantable medical device (AIMD), Cascaded heterogeneous equivalent network, Magnetic resonance imaging (MRI) safety, Transfer function, Transmission line model.**

I. Introduction

MAGNETIC resonance imaging (MRI) has become a common diagnostic tool since it is non-invasive and can provide quality images for soft tissues. However, it also leads to safety concerns for those patients with electrically long active implantable medical devices (AIMDs). One of the major concerns is the safety related to radiofrequency (RF)-induced energy. The induced RF energy deposited at the lead-tip can cause high localized temperature rise, leading to tissue injury. The voltage induced in the implantable pulse generator (IPG) may lead to functional damage of the AIMDs [1]-[7].

The transfer function method can be used to evaluate these safety concerns [8][9]. This technique divides the evaluation procedure into two independent parts: human body modeling and device characterization. Human body modeling involves the simulation of incident electric (E)-field distribution in numerical models of various human body types, exposed to MRI RF electromagnetic fields from various RF coil models, and the extraction of the tangential component of the incident E-field distributions along the AIMD implantation trajectories; Device characterization involves the development of AIMD models through measurement or numerical simulation [10]-[13]. The AIMD models together with the incident electric field are then used together to evaluate the RF-induced heating in tissue or induced voltage in the AIMDs. This technique substantially improves the efficiency and accuracy of RF compatibility evaluation for AIMDs in MRI.

In [13]-[19], the transmission line models were used for AIMD model development. In [16], Liu constructed the transmission line model by extracting two basic parameters, k_z and Z_0, for lead constructs with different sizes and dielectric constant of the insulator. However, these parameters were developed by immersing the leads' body into a homogeneous and infinitely large tissue-stimulating medium. For AIMDs in human tissue, such as a deep brain stimulation (DBS) system, the lead pathway travels through highly heterogeneous regions [20]. Therefore, such a homogeneous transmission line model may not be suitable. Current approaches of AIMD model development have two significant limitations:

1. The AIMD models are mostly developed in a homogeneous medium while clinically relevant pathways can have different tissue distributions along the lead body. Hence, one homogeneous AIMD model may not accurately represent the actual AIMD models for different pathways.
2. AIMD models need to be developed for each lead length. That is, if an IPG is used together with four different lead lengths, four different AIMD models need to be measured and validated.

A transfer function measurement setup in cascaded media is present in [21], but it only considered cases where the device is partially inside and partially outside a phantom. In this paper, a cascaded heterogeneous equivalent network is proposed to

Corresponding author: Ji Chen. J. Liu, Y. Wang, R. Guo, Q. Wang, J. Zheng, and J. Chen are with the Department of Electrical and Computer Engineering, University of Houston, Houston, TX 772044005 USA (e-mail: jliu44@uh.edu; ywang129@uh.edu; guoran188@gmail.com; qwang25@uh.edu; jzheng4@central.uh.edu; jchen23@central.uh.edu).

Krishna N. Kurpad is with Micro systems Engineering, Inc, Lake Oswego, OR, 97035, USA (krishna.kurpad@biotronik.com).

W. Kainz is with the Center for Devices and Radiological Health, Food and Drug Administration, Rockville, MD 20852 USA (e-mail: wolfgang.kainz@fda.hhs.gov).

address these concerns for AIMDs implanted in an anatomically correct human body model.

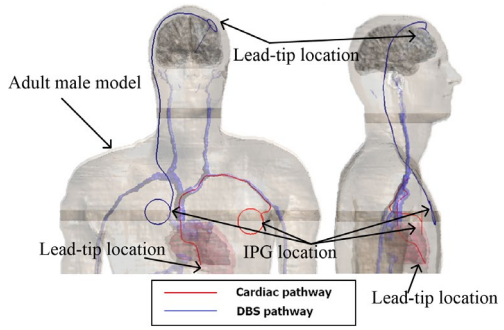

Fig. 1. Implantation pathways of cardiac and DBS devices.

This network consists of three parts: 1) IPG impedance, 2) lead-tip impedance, and 3) segmented transmission line with equivalent k_z and Z_0 along clinically relevant pathways. Using this approach, one can readily build models of AIMDs implanted along inhomogeneous tissue pathways by cascading multi-segment transmission line models. In addition, for AIMDs with the same lead body construct, one can easily develop AIMD models for different lead lengths. This approach can potentially enable the fast development of accurate and clinically relevant AIMD models.

The remainder of the paper is organized as follows: In Section II, the development of the cascaded transmission line network of the AIMD is presented. Methods to extract the IPG and lead-tip impedance, k_z and Z_0 for lead body in the inhomogeneous medium are also described. In Section III, the extraction of model parameters and their validation by numerical simulation for two simplified AIMDs are presented. Based on the extracted model parameters, unique models of the same AIMD implanted along different lead pathways or AIMDs of different lengths but having the same body construct are presented. Section IV gives the experimental validation of this method using simplified AIMD models. The discussion is made in Section V. The conclusion is drawn in Section VI.

II. METHODOLOGY

A. Cascaded transmission line model

Fig. 1 shows two implantation trajectories of AIMDs inside a human body model for cardiac and DBS applications inside the adult male model from virtual family [22]. To illustrate the development of the cascaded AIMD models, the tissues surrounding a DBS lead pathway are extracted and shown in Fig. 2(a).

When the lead body structures are implanted inside the inhomogeneous medium, the whole system can be considered as a cascade of transmission line segments as shown in Fig. 2 (b). The electrical parameters of each transmission line segment are related to the lead construct as well as the tissues surrounding that segment. Using this cascaded transmission line model, the transfer function model (also referred to as the AIMD model) can be extracted using the reciprocity approach [9]. For example, if the voltage transfer function for an AIMD model is required, a localized current source I_s should be applied at the IPG side, so Z_s stands for the impedance of IPG, while Z_L represents the impedance of the lead-tip. Each segment of the lead body is now surrounded by different tissues and would have different k_z and Z_0 values. The induced current distribution, $I(l)$ along the transmission line is equivalent to the transfer function model to be determined.

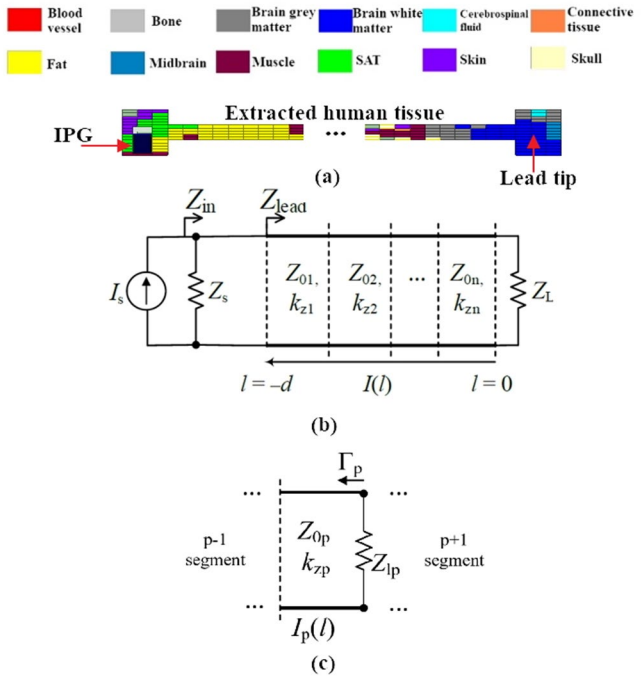

Fig. 2(a) Simplified simulation model for an AIMD implanted in heterogeneous human tissues (b) cascaded heterogeneous equivalent network.

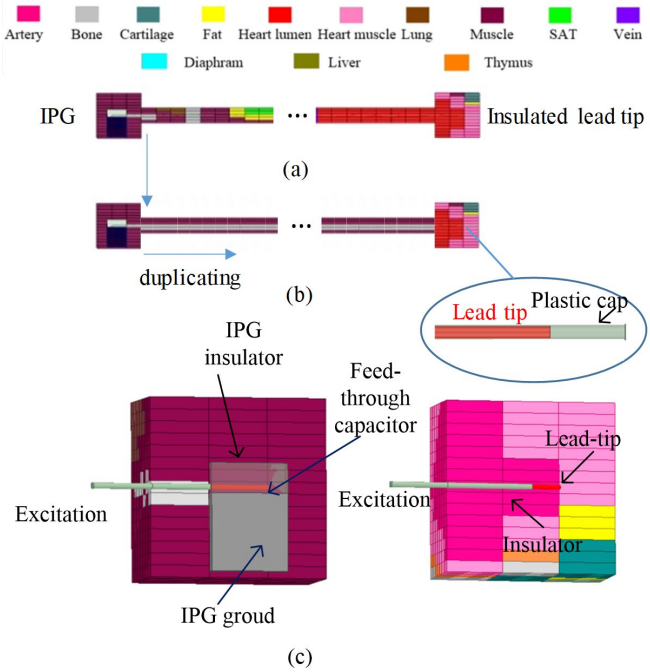

Fig. 3(a) Model to extract k_{zp} and Z_{0p}. The excitation is applied on the IPG, and the lead-tip is insulated. (b) Extracting the first segment of the lead body together with its surrounding media and duplicating along the positive z-direction. (c) model to extract IPG impedance and lead-tip impedance

To evaluate the induced current $I(l)$ based on the transmission line model, a recursive method or any transmission line solver, such as SPICE, can be used. Consequently, as long as the IPG input impedance, the lead-tip impedance, and the wave number/characteristic impedance for each segment of the lead body in tissues are known, the AIMD model can be determined.

B. Evaluation of the parameters

The evaluation of the k_{zp} and Z_{0p} for p-th segment surrounded by different tissues can be achieved through numerical modeling. To determine k_{zp} and Z_{0p}, (the wavenumber and characteristic impedance of the p-th segment of the cascaded transmission line model), the p-th segment of the lead body together with its surrounding media are selected and duplicated along the entire lead body, as shown in Fig. 3(a)(b). A plastic cup was placed on the lead-tip so that the lead-tip is now considered as an open-ended termination. The excitation is applied to the internal circuit of IPG. The curve fitting method is applied in the determination of k_{zp} [8][9]. The fitting function is

$$f(l) = e^{-jk_{zp}(d-l)}(1 - \Gamma_{open}e^{-2jk_{zp}l}) \quad (1)$$

where k_{zp} is the wavenumber of p-th segment to be determined (the only unknown), $\Gamma_{open} = 1$ due to the insulation of the lead-tip, d is the total length of the lead, and l is the distance to the excitation. The fitting data is the transfer function, $TF(l)_{p,sim}$, extracted from simulation shown in Fig. 3(b). Then, the characteristic impedance Z_{0p} for this segment can be calculated by

$$Z_{0p} = Z_{in,p}\frac{1-\Gamma_{open}e^{-2jk_{zp}d}}{1+\Gamma_{open}e^{-2jk_{zp}d}}. \quad (2)$$

where $Z_{in,p}$ is the impedance of looking into the lead body from the excitation port, which can be easily extracted from simulation.

The IPG and the lead-tip are modeled as lumped elements as described in [13]-[16]. IPG input impedance is related to the internal design of the AIMD system and the lead-tip impedance is associated with the energy deposition inside the tissue surrounding the lead-tip. Both of the IPG input impedance and lead-tip impedance can be derived from measurement or numerical simulation as shown in Fig. 3 (c). To obtain the input impedances for IPG and lead-tip, the tissues surrounding the IPG or lead-tip are extracted. An ideal coax cable is used as excitation to extract the input impedance, i.e., the IPG or lead-tip impedance [16]. Once all these parameters are extracted, one can build the overall AIMD models based on the cascaded transmission line network illustrated in Fig. 2 (b).

III. SIMULATION RESULTS

AIMD models for the cardiac pathway and DBS pathway shown in Fig. 1 were developed in this section through numerical modeling using ANSYS HFSS 2018.0. The human body model used in this study is the Duke model from the virtual family project [21]. The AIMD models were developed for 1.5 T MRI system.

Each study is divided into two parts: (1) Extracting IPG, lead-tip impedance, and k_z, Z_0 distribution; (2) Building AIMD models based on cascaded transmission line model.

A. Extracting IPG, lead-tip impedance, and k_z, Z_0

1) Cardiac pathway: As shown in Fig. 1, the cardiac IPG was implanted in the regions of the muscle and fat tissues, with a small portion of the lead body implanted between these two tissues. The remaining portion of the lead was placed in the vein, leading into the heart. The total length of the cardiac pathway was 75 cm. The simplified lead constuct with single straight conductor was applied in this study to demonnstrate this approach. The radii of the lead conductor and the insulator were 0.4 mm and 0.5 mm, respectively. The relative permittivity of the lead insulator was 3.5. The length of the bare lead-tip was 5 mm. The tissue surrounding the IPG and the lead is modeled by small boxes with dimension of 2 mm×2 mm×10 mm (in the direction tangent to the lead). The cross-section of the tissue tube along the lead body is 1 cm×1 cm. The material around the tissue boxes and AIMD is the saline with a dielectric constant of 78 and conductivity of 0.47 S/m. The simulation frequency is 64 MHz.

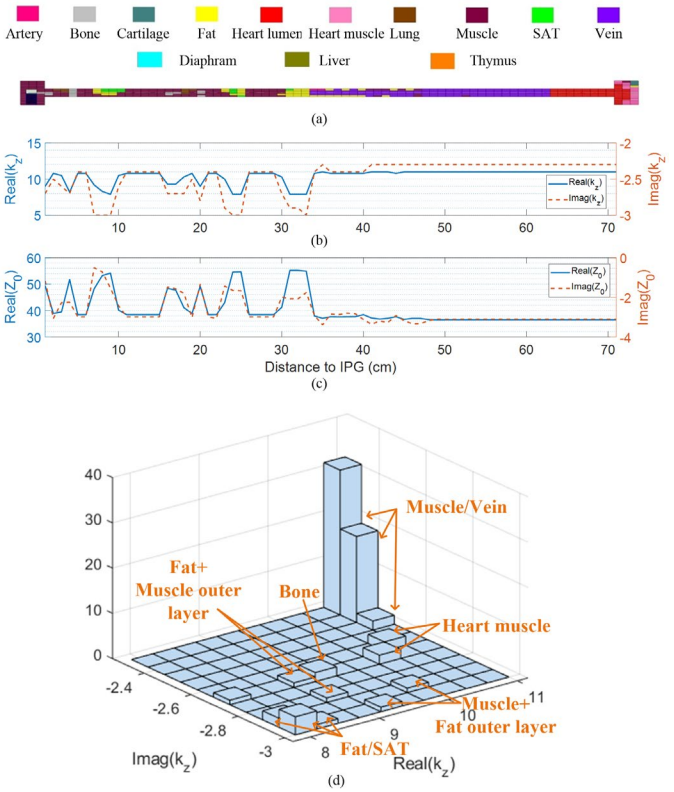

Fig. 4(a) Simulation model to k_z and Z_0 for the cardiac pathway study (b) k_z and (c) Z_0 distribution along the cardiac device; (d) the distribution of k_z values for different segments of the lead (Fat+Muscle outer layer means the lead passes through the fat, and surrounded by the muscle outer layer)

TABLE I
THE IMPEDANCE OF IPG AND LEAD-TIP OF CARDIAC DEVICE

PATHWAY	IPG (Ohm)	LEAD-TIP (OHM)
Cardiac	18.4 - 0.9i	97.3 - 51.7i

TABLE II
k_z, Z_0 OF LEAD BODY V.S. TISSUES NEAR THE LEAD FOR CARDIAC DEVICE

Tissue	Mean of Z_0 (Ohm)	Mean of k_z
Muscle/Vein	39.1 - 2.7i	10.7 - 2.4i
Heart muscle	38.2 + 0.1i	10.4 – 2.2i
Muscle+Fat outer layer	43.0 - 1.4i	10.0 - 2.9i
Fat+Muscle outer layer	48.4 - 1.5i	9.3 - 2.7i
Bone	49.3 - 1.5i	8.9 - 2.7i
Fat/SAT	53.7 - 1.4i	8.1- 2.9i

The IPG and lead-tip impedances were extracted from two independent simulations, of which the numerical models were shown in Fig. 3 (c). In both simulation models, the lead body was replaced by an ideal coax cable excited by a wave port. From Fig. 3 (c), the IPG was surrounded by muscle and a small portion of fat; while the tissues surrounding the lead-tip, shown in Fig. 3 (c), were mainly heart lumen and heart muscle. The IPG and lead-tip impedances can be extracted from the Z matrix in the solution files of simulations. The extracted impedance of IPG and lead-tip of the cardiac device was shown in Table I.

The simulation model to extract k_z, Z_0 is shown in Fig. 4(a). The waveport excitation is added in the IPG. The lead-tip is capped by the insulation material. The current distribution along the lead (i.e. the transfer function $TF(l)_{p,sim}$) and the input impedance at the excitation $Z_{in,p}$ can be derived. Based on the (1) and (2), the k_{zp}, Z_{0p} distribution along the cardiac trajectory was determined, and shown in Fig. 4(b)(c). To directly analyze the relation between the tissue near the lead body and the corresponding k_z, Z_0 value, the 2D-distribution of k_z verses the passing tissue is plotted in Fig. 4 (d).

In this figure, one can find that there are six clusters of the extracted k_z value. The k_z, Z_0 was related to surrounding tissue that the lead body travels through since most energy of the guided-wave was confined around the insulator [13]-[16]. It was obvious that the effective k_z, Z_0 values were significantly different between high-loss media, dominated by muscle, vein or heart muscle, and low-loss media, dominated by fat, Subcutaneous Adipose Tissue (SAT). The outer tissue layer surrounding the lead body but does not have direct contact with the lead body also affects k_z, Z_0. For example, for the lead segments surrounded by muscle and further encaspulated by another by fat layer (see notation Muscle+Fat outer layer), the real part of k_z would be smaller than that surrounded by muscle layer only but still larger than that surrounded by fat layer only. Based on this argument, the relationship between the tissue near the lead body and the mean value of k_z, Z_0 were summarized in Table II.

2) DBS pathway: From Fig. 1, the DBS IPG has lead body pathways traveling through fat, SAT, muscle, conductive tissue, and brain grey matter, and finally reaches brain white matter. The total length of the DBS pathway was 100 cm. The lead body and IPG used here were the same as those used in the cardiac pathway study. The simulation model to extract k_z, Z_0 is shown in Fig. 5(a).

The extracted impedance of IPG and the lead-tip of the DBS device was shown in Table III. Based on the (1) and (2), the k_z, Z_0 distribution along the DBS trajectory was determined, and shown in Fig. 5(b)(c). Again, values for both characteristic impedance and wavenumber along the pathway can have significant variations in low loss (Fat, SAT, etc.) and high loss media (Muscle, vein, etc.). The 2D-distribution of k_z verses the passing tissue is plotted in Fig. 5(d). one can find that there are five clusters of the extracted k_z value. The relationship between the tissue near the lead and the mean value of k_z, Z_0 were summarized in Table IV.

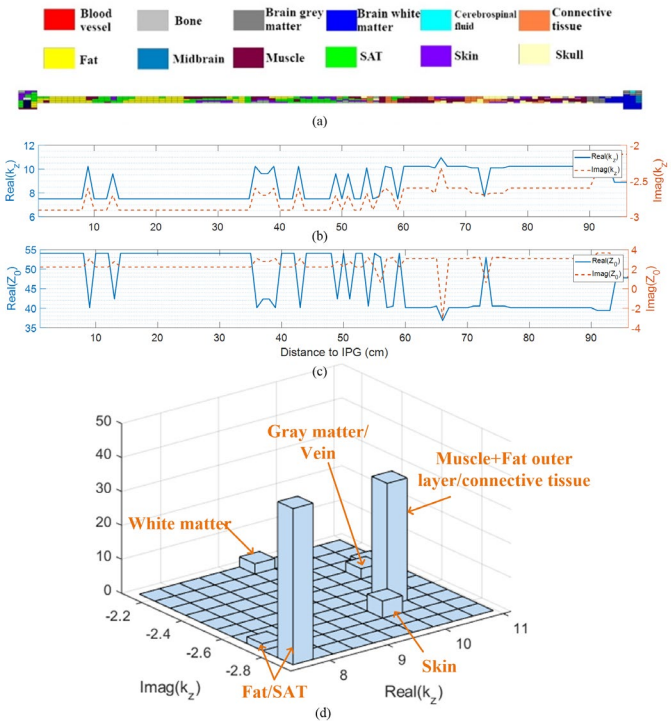

Fig. 5 (a) Simulation model to k_z and Z_0 for the DBS pathway study (b) k_z and (c) Z_0 distribution along the DBS device; (d) the distribution of k_z values for different segments of the lead.

TABLE III
THE IMPEDANCE OF IPG AND LEAD-TIP OF DBS DEVICE

PATHWAY	IPG (Ohm)	LEAD-TIP (OHM)
DBS	36.8 - 13.6i	118.3 - 113.7i

TABLE IV
k_z, Z_0 OF LEAD BODY V.S. TISSUES NEAR THE LEAD FOR DBS DEVICE

Contacting Tissue	Mean of Z_0 (Ohm)	Mean of k_z
Fat/SAT	54.0 + 2.2i	7.4 - 2.9i
White matter	47.7 - 2.1i	8.8 - 2.1i
Skin	42.3 + 2.7i	9.6 - 2.7i
Muscle+Fat outer layer/Connective tissue	40.5 + 3.1i	10.1 - 2.6i
Vein/ Grey matter	39.6 + 4.1i	10.5 - 2.6i

B. AIMD models based on cascaded transmission line model

Based on the cascaded transmission line model and the extracted parameters, AIMD models can be developed. A MATLAB script based on the recursive method was used to develop the AIMD models. The magnitudes and phases of AIMD models for RF-induced heating and RF-induced voltage were presented in Fig. 6. For the RF-induced heating transfer functions, the excitation is at the lead-tip, and the load is the IPG. The transfer function is extracted from the lead-tip to IPG.

For the RF-induced voltage transfer functions, the excitation is at the IPG, and the load is the lead-tip. The transfer function is extracted from the IPG to the lead-tip. Also, the AIMD models for the pathways shown in Fig. 4(a) and Fig. *5*(a) were also extracted using full-wave simulation and results are also shown in Fig. 6.

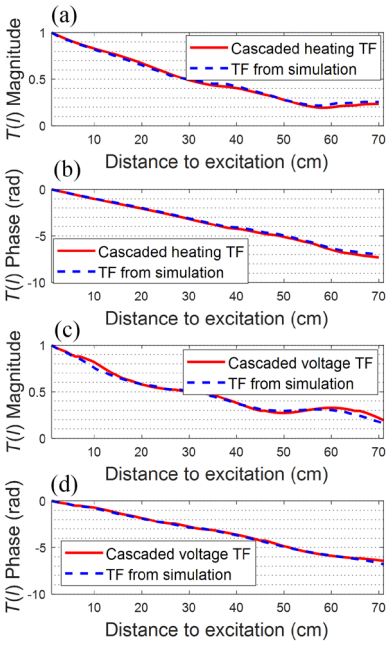

Fig. 6 Comparison of heating transfer functions in (a), (b) and voltage transfer functions (TFs) in (c), (d) of cardiac pathway between cascaded model and direct simulation.

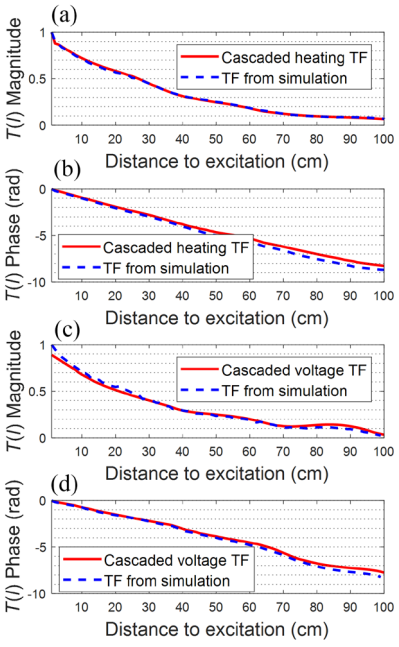

Fig. 7 Comparison of heating transfer functions in (a), (b) and voltage transfer functions(TFs) in (c), (d) of DBS pathway between cascaded model and direct simulation.

It was evident that transfer functions from the cascaded model and direct simulation agreed very well with each other. The comparison of AIMD models for the DBS pathway developed using the proposed approach and the direct full-wave methods as shown in Fig. 7 also showed good agreement. This further validated the accuracy of the cascaded transmission line method for the AIMD model development. It should be pointed out that in the full-wave transfer function extraction, one needed to extract the AIMD model for each pathway configuration while the cascaded transmission line approach can generate AIMD models for arbitrary pathways using the parameters presented in previous tables.

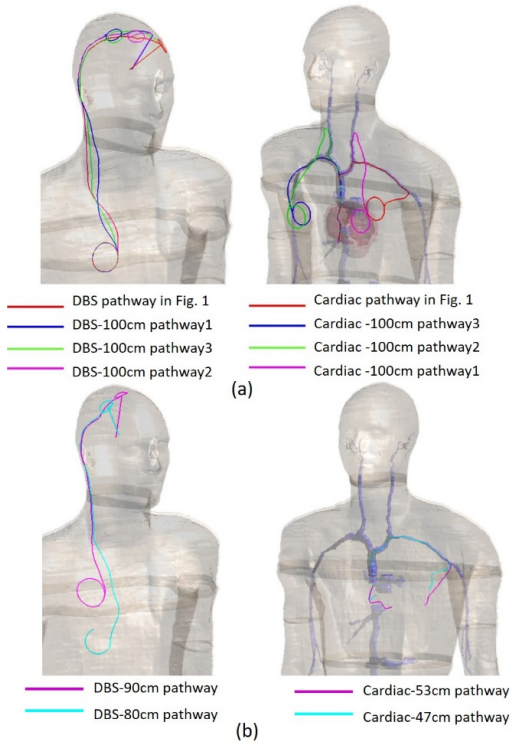

Fig. 8 Implantation pathways used for prediction of voltage transfer functions both for cardiac and DBS devices, (a) pathways with identical length as the example pathways in Fig. 1, (b) pathways with different lengths but same AIMD construct.

C. AIMD models for arbitrary cardiac and DBS pathways

As mentioned in the previous section, using the parameters in Table I to Table IV, one can develop AIMD models for arbitrary inhomogeneous pathways for different lead body length. Fig. 8 (a) showed three possible implantation pathways for DBS and cardiac devices whose lengths were 100 cm. Fig. 8 (b) gives clinical implantation cases of DBS and cardiac devices which have different lengths. Since these pathways all have the same starting and ending locations, the IPG and lead-tip impedance would be the same but the k_z, Z_0 distributions along different pathways can be different.

With the k_z, Z_0 in Table II and Table IV and lead-tip and IPG impedances in Table I and Table III, the voltage AIMD models for the cardiac and DBS pathways in Fig. 8 can be generated using the recursive method, as shown in Fig. 9. The differences among the AIMD models of the three pathways with equal length indicated that it was necessary to build individual AIMD models for each pathway. This will provide implantation

specific AIMD model for both RF-induced heating and RF-induced voltage.

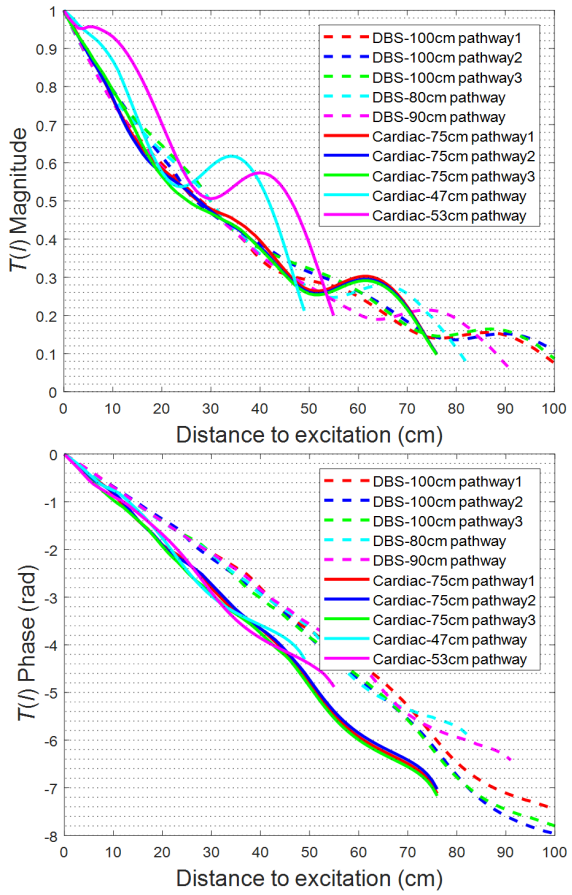

Fig. 9 The magnitude and phase of the voltage transfer functions (TFs) for five DBS and cardiac pathways

IV. MEASUREMENT VALIDATION

The measurement was also performed to validate the effectiveness of the cascaded heterogeneous equivalent network for AIMDs in heterogeneous media. The validation procedure was divided into two parts: (1) experimentally extracting the k_z, Z_0 for the lead body immersed in the saline with different conductivity, and the impedance of IPG and lead-tip; (2) Comparing the developed AIMD model using cascaded transmission line network with that measured in a heterogeneous phantom consisting of three compartments of salines with different conductive values.

A. Extracting the parameters

The device used in the experimental validation was a simplified AIMD which consists of a dummy IPG and insulated solid wire with a bare lead-tip on the distal end, as shown in Fig. 10. The IPG had a copper sheet as metallic case, and a soldered 2.1 Ohm resistor acting as the internal impedance of the IPG, which was insulated by plastic adhesive. The lead body was made of a conductor and insulator with 0.4 mm and 0.8 mm radius, respectively. The length of the bare lead-tip was 5 mm. The total lead length of the device was 45 cm. This device was immersed into three salines with conductivities of 0.3 S/m, 0.65 S/m, and 1.2 S/m, and relative permittivity of 78 at 64 MHz to extract the k_z, Z_0 in each medium. Similar to numerical simulation, during the extraction of the k_z, Z_0, the distal end of lead should be insulated to keep $\Gamma_{open} = 1$ in (1) and (2). The k_z, Z_0 values were extracted using the curve fitting algorithm described earlier.

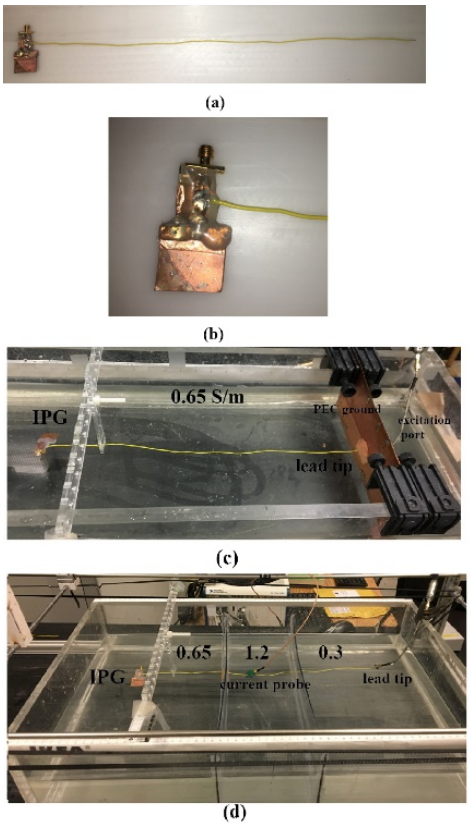

Fig. 10(a) Simplified AIMD and (b) its dummy IPG, soldered with a resistor of 2.1 ohm; (c) experimental platform to extract the impedance of IPG and (d) heterogeneous phantom for AIMD model development.

TABLE V
MEASURED k_z, Z_0, AND THE IMPEDANCE OF IPG AND LEAD-TIP

CONDUCTIVITY (S/M)	K_Z	Z_0(OHM)	IPG(OHM)	Lead-tip (OHM)
0.3	5.3-0.6i	95.3-8.8i		
0.65	6.1-0.9i	72.9+2.0i	23.3-1.0i	182.0+90.8i
1.2	5.8-0.6i	88.2-18.7i		

In the measurement, IPG impedance can be estimated through measurement by placing the entire system under gel with 0.65 S/m conductivity. The lead-tip was directly connected to a vector network analyzer (VNA) to measure the overall impedance as shown in Fig. 10 (c). With the obtained input impedance and known k_z, Z_0 parameters extracted for 0.65 S/m, the IPG input impedance was estimated as

$$Z_{IPG} = \frac{Z_0^2 \tanh(jk_z d) - Z_{in} Z_0}{Z_{in} \tanh(jk_z d) - Z_0} \quad (3)$$

where d was the length of the lead. A similar approach can be used for the electrode tip impedance extraction. The measured k_z, Z_0 in each medium, and the impedance of IPG and lead-tip were shown in Table V.

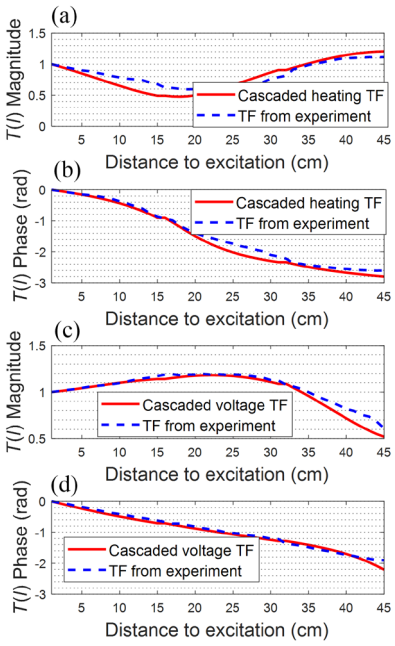

Fig. 11. Comparison of heating transfer functions (TFs) in (a), (b) and voltage transfer functions in (c), (d) derived from cascaded transmission line model and direct measurement in the heterogeneous phantom.

B. Comparison of AIMD models

Once these parameters were determined, the heterogeneous AIMD model could be developed based on the recursive method. Also, the directly measured AIMD model was presented to show the validity of the cascaded result. Fig. 10(d) showed the set up for the heterogeneous AIMD model heating model development. As the current probe moved along the lead body, the AIMD model was recorded by the VNA [9]. The length of each segment in the saline with various conductivities was 15 cm. Similarly, the AIMD model for the induced voltage transfer function was also developed. The comparison of AIMD models derived from the cascaded transmission line model and direct measurement in the heterogeneous phantom were shown in Fig. 11, which showed a close match for both heating and voltage transfer functions. That indicated the validity of the proposed cascaded heterogeneous equivalent network.

The uncertainty of the measurement can be divided into two parts: the measurement of wavenumber and the charastistic impedance. Using the same method applied in [23], the uncertainty from these two sources is 1.9% and 5.0%, respectively. Therefore, the combined uncertainty for the measurement is 5.3%.

V. Discussion

To demonstrate the advantages of the proposed cascaded transmission line model, we perform a comparative study. The RF-induced heating transfer function derived by the cascaded transmission line model for the DBS pathway is compared to those derived using the Tier 3 approach in ISO 10974. High permittivity medium (HPM) with a conductivity of 0.47 S/m, relative permittivity of 78, and the low permittivity medium (LPM) with a conductivity of 0.05 S/m, relative permittivity of 15 are used. The same AIMD system used for the DBS pathway study is placed in HPM and LPM to derive the transfer functions and compared to the simulated transfer function when the AIMD system is in the heterogeneous tissue (consided as the true model) as shown in Fig. 5(a).

The result is shown in Fig. 12. We can see that the transfer function derived from the cascaded transmission line model has a closer match with the simulated transfer function in the heterogeneous tissue compared to the transfer functions derived in LPM and HPM. To numerically analyze the difference between the cascaded transfer function and other transfer functions, we calculate the error and present it in TABLE VI. $\mathbf{TF}_{sim}$ is the complex vector of simulated transfer function of the AIMD in the heterogeneous tissue, $\mathbf{TF}_{model}$ is the complex vector of the transfer function derived in LPM, HPM or the cascaded transfer function (proposed method). We can see that the cascaded transfer function has the minimum error compared to the transfer functions derived in the LPM and HPM.

From this study, the major advantage is the accuracy compared to the approached in ISO 10974. It can develop a unique model for any AIMDs with arbitrary implantation trajectories in the human model. That will improve the accuracy of the RF-induced heating and voltage evaluation.

However, the simplified lead model is used in this paper, which is a limitation of this study. For the realistic leads, the simulation time will be longer due to the complicated lead structure. Also the accuracy of the proposed approach for the real lead needs to be studied in the future. In the experiment, only the straight trajectory is considered. More configuration of the lead-tip in the phantom should be studied in the future.

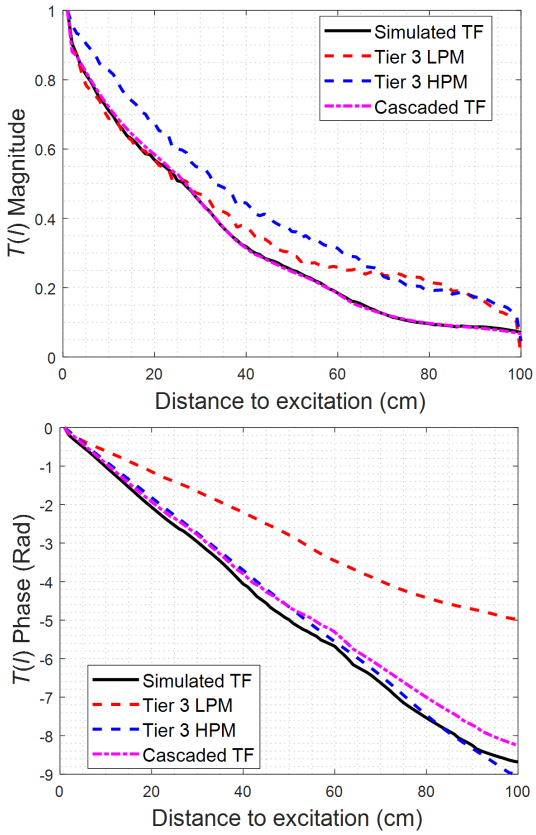

Fig. 12. Comparison of transfer functions (TFs) derived from cascaded transmission line model and ISO 10974 Tier 3 approach using low permittivity

medium (LPM) and high permittivity medium (HPM) with the simulated transfer function in the heterogeneous tissue.

TABLE VI.

THE ERROR BETWEEN THE SIMULATED TF IN THE HETEROGENEOUS TISSUE AND OTHER TFS DERIVED BY DIFFERENT APPROACHS.

	$error = \frac{\|\mathbf{TF}_{sim} - \mathbf{TF}_{model}\|}{\|\mathbf{TF}_{sim}\|}$
Tier 3 LPM	1.06
Tier 3 HPM	0.36
Cascaded TF	0.17

VI. CONCLUSION

This paper presents a cascaded transmission line method for the determination of the electromagnetic model of AIMD implanted in the inhomogeneous human body and exposed MRI RF electromagnetic fields. It can develop a unique model for any AIMDs with arbitrary implantation trajectories. Different trajectories may have different equivalent networks since the tissue distribution along the lead might not be similar. The cascaded heterogeneous equivalent network is more accurate and efficient to evaluate RF-induced heating and RF-induced voltage.

VII. DISCLAIMER

The mention of commercial products, their sources, or their use in connection with material reported herein is not to be construed as either an actual or suggested endorsement of such products by the Department of Health and Human Services.

REFERENCES

[1] R. Kalin and M. S. Stanton, "Current clinical issues for mri scanning of pacemaker and defibrillator patients," *Pacing and clin. Electrophysiol.*, vol. 28, no. 4, pp. 326–328, 2005.

[2] S. Nazarian, R. Hansford, A. Roguin, D. Goldsher, M. M. Zviman, A. C. Lardo, B. S. Caffo, K. D. Frick, M. A. Kraut, I. R. Kamel, *et al.*, "A prospective evaluation of a protocol for magnetic resonance imaging of patients with implanted cardiac devices," *Annals of intern. Med.*, vol. 155, no. 7, pp. 415–424, 2011.

[3] E. Neufeld, S. Kuhn, G. Szekely, and N. Kuster, "Measurement, simula-¨ tion and uncertainty assessment of implant heating during mri," *Phys. in Med. & Biol.*, vol. 54, no. 13, p. 4151, 2009.

[4] E. Cabot, E. Zastrow, and N. Kuster, "Safety assessment of aimds under mri exposure: Tier3 vs. tier4 evaluation of local rf-induced heating," in *Electromagn. Compat., Tokyo (EMC'14/Tokyo), 2014 Int. Symp. On Electromagn. Compat.*, pp. 237–240, IEEE, 2014.

[5] H. Irak, *Modeling RF heating of active implantable medical devices during MRI using safety index*. PhD thesis, Dept. of Elect. and Electron. Eng. and the Inst. of Eng. and Sci. of Bilkent Univ., 2007.

[6] ASTM-F2182-11a, "Standard test method for measurement of radio frequency induced heating on or near passive implants during magnetic resonance imaging, astm international," 2011.

[7] R. Luechinger, V. A. Zeijlemaker, E. M. Pedersen, P. Mortensen, E. Falk, F. Duru, R. Candinas, and P. Boesiger, "In vivo heating of pacemaker leads during magnetic resonance imaging," *Eur. heart J.*, vol. 26, no. 4, pp. 376–383, 2004.

[8] S.-M. Park, R. Kamondetdacha, and J. A. Nyenhuis, "Calculation of mri-induced heating of an implanted medical lead wire with an electric field transfer function," *J. Magn. Reson. Imag.*, vol. 26, no. 5, pp. 1278–1285, 2007.

[9] S. Feng, R. Qiang, W. Kainz, and J. Chen, "A technique to evaluate mri-induced electric fields at the ends of practical implanted lead," *IEEE Trans. on Microw. Theory and Techn.*, vol. 63, no. 1, pp. 305–313, 2015.

[10] J. Tokaya, A. Raaijmakers, P. Luijten, J. Bakker, and C. A. van Den Berg, "Mri-based transfer function determination for the assessment of implant safety," *Magn. Reson. in Med.*, vol. 78, no. 6, pp. 2449–2459, 2017.

[11] J. Liu, J. Zheng, Q. Zeng, Q. Wang, J. Rondoni, J. Olsen, W. Kainz, and J. Chen, "Investigations on *tissue*-simulating medium for mri rf safety assessment for patients with active implantable medical devices," *IEEE Trans. on Electromagn. Compat.*, no. 99, pp. 1–7, 2018.

[12] Y. Wang, Q. Wang, J. Liu, Q. Zeng, J. Zheng, W. Kainz, and J. Chen, "On the development of equivalent medium for active implantable device radiofrequency safety assessment," *Magn. Reson. Med.,* vol. 82, no. 3, pp. 1164–1176, 2019.

[13] M. Kozlov and W. Kainz, "Lead electromagnetic model to evaluate RF-induced heating of a coax lead: A numerical case study at 128 mhz," *IEEE J. of Electromagn., RF and Microw. in Med. and Biol.*, 2018.

[14] V. Acikel and E. Atalar, "Modeling of radio-frequency induced currents on lead wires during mr imaging using a modified transmission line method," *Med. Phys.*, vol. 38, no. 12, pp. 6623–6632, 2011.

[15] V. Acikel, A. Uslubas, and E. Atalar, "Modeling of electrodes and implantable pulse generator cases for the analysis of implant tip heating under mr imaging," *Med. Phys.*, vol. 42, no. 7, pp. 3922–3931, 2015.

[16] J. Liu, J. Zheng, Q. Wang, W. Kainz, and J. Chen, "A transmission line model for the evaluation of mri rf-induced fields on active implantable medical devices," *IEEE Trans. on Microw. Theory and Techn.*, vol. 66, no. 9, pp. 4271–4281, 2018.

[17] R. King, "Antennas in material media near boundaries with application to communication and geophysical exploration, part i: The bare-metal dipole," *IEEE Trans. on Antennas and Propag.*, vol. 34, no. 4, pp. 483–489, 1986.

[18] R. King, B. Sandler, and T. Wu, "Cylindrical antennas immersed in arbitrary homogeneous isotropic media," *J. of Appl. Phys.*, vol. 40, no. 13, pp. 5049–5065, 1969.

[19] T. W. Hertel and G. S. Smith, "The insulated linear antenna-revisited," *IEEE Trans. on Antennas and Propag.*, vol. 48, no. 6, pp. 914–920, 2000.

[20] J. S. Perlmutter and J. W. Mink, "Deep brain stimulation," *Annu. Rev. Neurosci.*, vol. 29, pp. 229–257, 2006.

[21] T. Lottner, S. Reiss, A. Bitzer, M. Bock, A. Ozen, "A Transfer Function Measurement Setup With an Electro-Optic Sensor for MR Safety Assessment in Cascaded Media", *IEEE Trans. on Electromagn. Compat.,* to be published.

[22] A. Christ, W. Kainz, E. G. Hahn, K. Honegger, M. Zefferer, E. Neufeld, W. Rascher, R. Janka, W. Bautz, J. Chen, *et al.*, "The virtual family development of surface-based anatomical models of two adults and two children for dosimetric simulations," *Phys. in Med. & Biol.*, vol. 55, no. 2, p. N23, 2009.

[23] Y. Wang, S. Song, J. Zheng, Q. Wang, S. Long, W. Kainz and J. Chen, "A novel device model validation strategy for 1.5- and 3-T MRI heating safety assessment," IEEE Trans. Instrum. Meas., vol. 69, no. 9, pp. 6381–6389, 2020.